Supporting Information

Synthesis and Catalytic Activity of Tridentate *N*-(2-Pyridylethyl)-Substituted Bulky Amidinates of Calcium and Strontium

Sven Krieck,*[a] Diana Kalden,[a] Ansgar Oberheide,[b] Lydia Seyfarth,[b] Hans-Dieter Arndt,[b] Helmar Görls,[a] and Matthias Westerhausen*[a]

Content

Catalytic Cyclohydroamination of 2,2-Diphenylpent-4-ene-1-amine

Preparative scale experiments: The used aminoalkene 2,2-diphenylpent-4-enylamine was prepared according to a literature protocol[1] and the purity was controlled by NMR spectroscopy. A solution of 4–5 mol-% precatalyst (**2c**, (*R*,*R*)-**2d**, (*S*,*S*)-**2d**) in C_6D_6 was added at r.t. to a solution of aminoalkene (89–144 mg, 0.37–0.61 mmol) in C_6D_6 and the conversion was monitored by ^{1}H NMR spectroscopy after taking of a sample. After complete conversion (**2c**: 4 mol-%, 18 h, 45 °C, 89%, (*R*,*R*)-**2d**: 5 mol-%, 7 d, r.t., 88%; (*S*,*S*)-**2d**:4 mol-%, 4 d, r.t., 87%) the reaction mixture was diluted with water (2–5 ml) and extracted with DCM. The organic layer was separated, dried over Na_2SO_4 and all volatiles were removed *in vacuo*. Subsequent purification by column chromatography (EtOAc/*n*-hexane/TEA 2:1:0.5) yielded the pyrrolidine derivative as yellow liquid. The resulting enantiomeric ratio was determined by chiral HPLC (Chiralcel® O*J*, *n*-hexane/EtOH 9:1, 0.1% add. DEA, 3 ml/min, 265 nm).

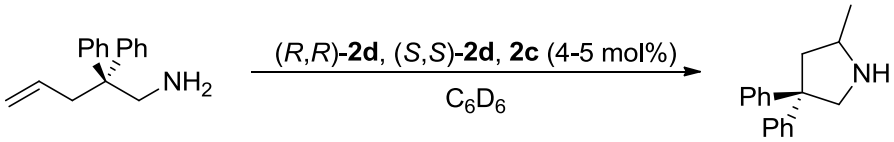

2,2-Diphenylpent-4-enylamine. B.p. 205 °C at $2.2 \cdot 10^{-2}$ mbar. ^{1}H NMR (C_6D_6, 297.0 K, 400.13 MHz): δ 7.12–7.07 (m, 8H, H_{ar}), 7.05–7.01 (m, 2H, H_{ar}), 5.50–5.40 (m, 1H, C*H*=CH$_2$), 5.01 (dt, *trans*-$^3J_{H,H}$ = 17.2 Hz, $^2J_{H,H}$ = 1.2 Hz, 1H, CH=CH_2), 4.92 (dt, *cis*-$^3J_{H,H}$ = 10.0 Hz, $^2J_{H,H}$ = 1.2 Hz, 1H, CH=CH_2), 3.16 (s, 2H, −CH_2NH$_2$), 2.86 (d, $^3J_{H,H}$ = 7.2 Hz, 2H, =CHCH_2−), 0.43 (s, br, 2H, −NH_2). ^{13}C{1H} NMR (C_6D_6, 297.0 K, 100.61 MHz): δ 147.2 (Ph *i*-*C*), 135.4 (*C*H=CH$_2$), 128.7 (C_{ar}), 128.3 (C_{ar}), 126.2 (C_{ar}), 117.6 (CH=*C*H$_2$), 51.5 (*C*Ph$_2$), 48.8 (−*C*H$_2$NH$_2$), 41.2 (=CH*C*H$_2$−).

2-Methyl-4,4-diphenylpyrrolidine. R_f (EtOAc/*n*-hexane/TEA 2:1:0.5, SiO$_2$) = 0.29. t_r = 11.81 min, 18.17 min (HPLC); *ee* = 0%. ^{1}H NMR ($CDCl_3$, 297.0 K, 400.13 MHz): δ 7.28–7.19 (m, 8H, H_{ar}), 7.17–7.12 (m, 2H, H_{ar}), 3.64 (dd, $^3J_{H,H}$ = 11.4 Hz, $^4J_{H,H}$ = 1.4 Hz, 1H, NH−CH_2), 3.45 (d, $^3J_{H,H}$ = 11.4 Hz, 1H, NH−CH_2), 3.37–3.30 (m, 1H, CH$_2$C*H*−CH$_3$), 2.71 (ddd, $^3J_{H,H}$ = 12.8 Hz, 6.6 Hz, $^4J_{H,H}$ = 1.6 Hz, 1H, CH−CH_2), 2.01 (dd, $^3J_{H,H}$ = 12.6 Hz, 9.0 Hz, 1H, CH−CH_2), 1.67 (s, br, 1H, N*H*), 1.18 (d, $^3J_{H,H}$ = 6.4 Hz, 3H, −CH_3). 13C{1H} NMR ($CDCl_3$, 297.0 K, 100.62 MHz): δ 148.0 (Ph *i*-*C*), 147.3 (Ph *i*-*C*), 128.5 (C_{ar}), 128.4 (C_{ar}), 127.2 (C_{ar}), 127.1 (C_{ar}), 126.1 (C_{ar}), 126.1 (C_{ar}), 58.1 (NH−*C*H$_2$), 57.5 (NH−*C*H$_2$), 53.3 (*C*Ph$_2$), 47.3 (CH−*C*H$_2$), 22.6 (−*C*H$_3$). ^{1}H NMR (C_6D_6, 297.0 K, 400.13 MHz): δ 7.21 (d, $^3J_{H,H}$ = 7.2 Hz, 2H, H_{ar}), 7.12–7.07 (m, 6H, H_{ar}), 7.03–6.99 (m, 2H, H_{ar}), 3.51 (ddd, $^3J_{H,H}$ = 11.0 Hz, 6.2 Hz, $^4J_{H,H}$ = 1.4 Hz, 1H, NH−CH_2), 3.33 (dd, $^3J_{H,H}$ = 11.0 Hz, 8.2 Hz, 1H, NH−CH_2), 3.19–3.09 (m, 1H, CH$_2$C*H*−CH$_3$), 2.38 (ddd, $^3J_{H,H}$ = 12.2 Hz, 6.4 Hz, $^4J_{H,H}$ = 1.2 Hz, 1H, CH−CH_2), 1.80 (dd, $^3J_{H,H}$ = 12.4 Hz, 9.2 Hz, 1H, CH−CH_2), 1.01 (d, $^3J_{H,H}$ = 6.4 Hz, 3H, −CH_3). HR-MS (GC-EI) calcd. for $C_{17}H_{20}N$ $[M+H]^+$: 238.1590 amu. Found: 238.1596 amu (error: 2.5 ppm).

Chiral Liquid Chromatography

Analyses were performed on a SHIMADZU system consisting of a system controller (SLC-10AVP), a column oven (CTO-10ACVP), an auto-injector (SIL-10ADVP), a degasser (DGU-14A), two pumps (LC-10ATVP), a diode array detector (SPD-M20A) and a UV-vis-detector (SPD-10AVP).

- For the analysis of the enantiomeric ratio of 2-methyl-4,4-diphenyl-pyrrolidine an isocratic flow (3 mL/min) of *n*-hexane/EtOH (90:10 v/v) containing 0.1% diethylamine and a CHIRALCEL® OJ column (250 × 10 mm ID, 10 µm, DAICEL) was used (method A).

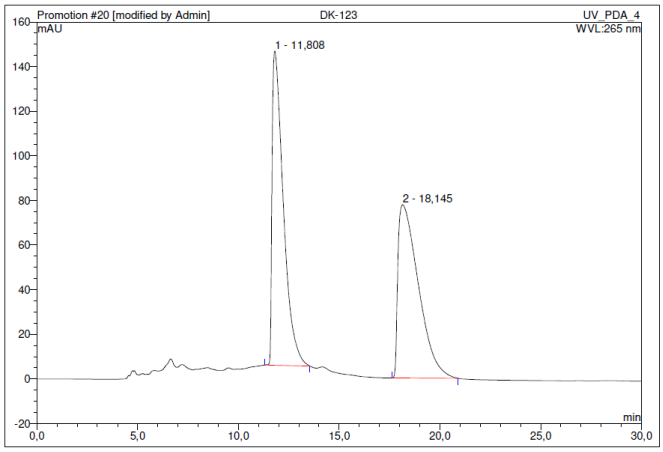

No.	Ret.Time min	Peak Name	Height mAU	Area mAU*min	Rel.Area %	Amount	Type
1	11,81	n.a.	140,756	91,040	49,90	n.a.	BMB*
2	18,15	n.a.	77,598	91,403	50,10	n.a.	BMB*
Total:			218,354	182,443	100,00	0,000	

Figure S1. Chiral HPLC trace of the racemic mixture of 2-methyl-4,4-diphenyl-pyrrolidine using method A.

- For the preparative separation of the racemic amidine **1d** an isocratic flow (6 mL/min) of *n*-hexane/EtOH (99.98:0.02 v/v) containing 0.1% diethylamine and a CHIRALPAK® IA column (250 × 20 mm ID, 5 µm, DAICEL) was used (method B).

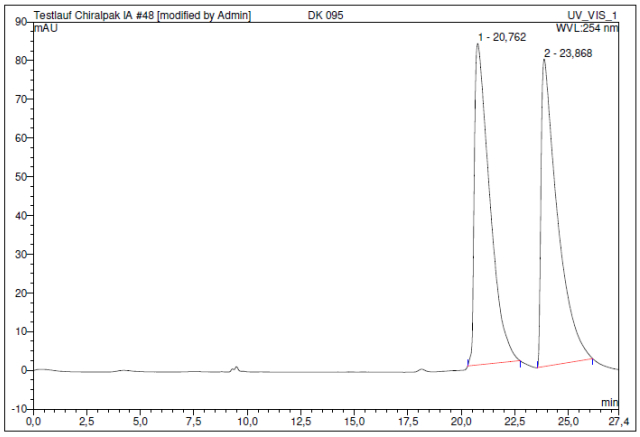

No.	Ret.Time min	Peak Name	Height mAU	Area mAU*min	Rel.Area %	Amount	Type
1	20,76	n.a.	82,986	69,083	49,60	n.a.	BMB*
2	23,87	n.a.	79,388	70,187	50,40	n.a.	BMB*
Total:			162,374	139,270	100,00	0,000	

Figure S2. Chiral HPLC trace of the racemic amidine **1d** using method B.

- The enantiopurity of both enantiomers of amidine **1d** was elucidated using an isocratic flow (1 mL/min) of *n*-hexane/EtOH (99.98:0.02 v/v) containing 0.1% diethylamine and a CHIRALPAK® IA column (250 × 4.6 mm ID, 5 µm, DAICEL) (method C).

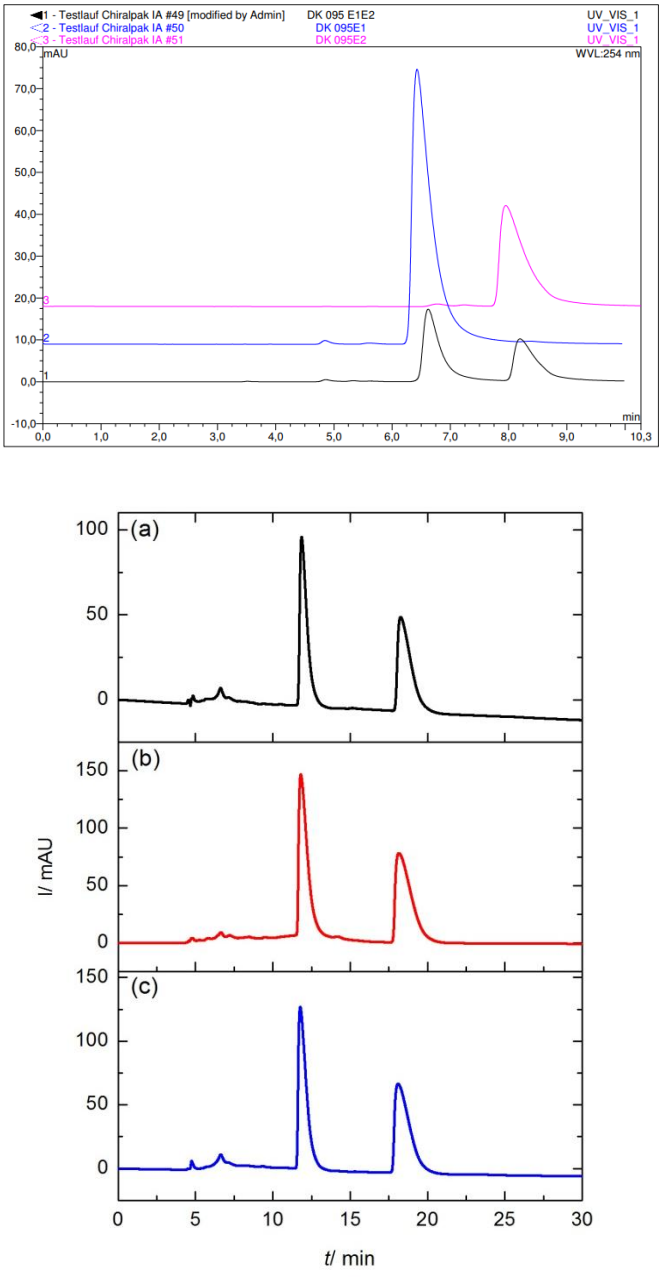

Figure S3. **Top**: Chiral HPLC traces of the racemic mixture of amidine **1d** (black) and both enantiomers (R)-**1d** (blue) and (S)-**1d** (purple) after separation, using method C. **Bottom:** Chromatographic separation of (R)- and (S)-2-methyl-4,4-diphenylpyrrolidine with chiral HPLC methods using the eluent n-hexane/ethanol with a ratio of 9:1. At the top 4 mol-% of complex **2c** was used as precatalyst for the hydroamination (a, 45 °C, 18 h, conversion of 89 %), in the middle and at the bottom, the chiral complexes (R,R)-**2d** (b, room temperature, 7 days, 88 %) and (S,S)-**2d** (c, room temperature, 4 days, 87 %) were applied.

NMR scale experiments for kinetic studies: In a typical experiment, an NMR sample was prepared using standard Schlenk techniques. The Youngs tap NMR tube was filled with 0.11 mmol of aminoalkene, 0.31 mmol of $(Me_3Si)_4Si$ (TMSS, 0.10 ml of a 0.031 M standard solution in C_6D_6) as internal standard and 2, 3, and 4 mol-%, respectively, of a standard solution of the appropriate precatalyst [({$Me_3Si)_2N$}Ca{Dipp−N=C(*t*Bu)N−C_2H_4−Py}] (**2c**), Eq. S1).[2]

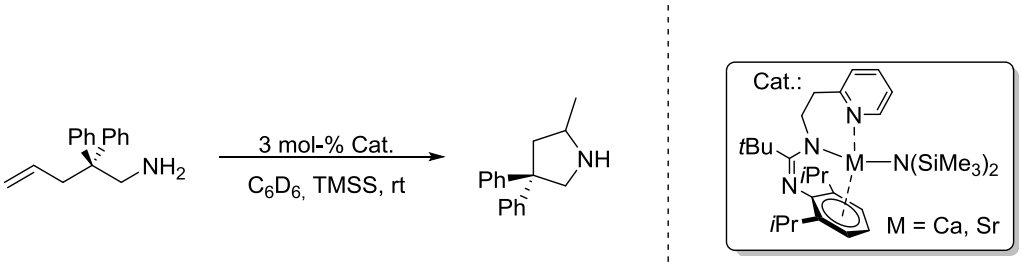

Eq. S1

The volume was filled up immediately to 0.45 ml with C_6D_6 and instantly frozen to 196 K and thawed just before the transfer into an Avance 400 Bruker NMR spectrometer. The NMR samples were then measured at preset temperatures of 10, 12, 24, 40, and 50 °C and data were acquired every 30 min in the case of catalyst concentration-dependent experiments and every 10 min in the case of temperature dependent experiments using 8 scans min^{-1}, a pulse delay of 8 s and 2D experiments. The conversion to the heterocyclic product was followed by integration of ^{1}H NMR spectra and the concentrations were determined by the signal intensities of the substrate with respect to the internal standard TMSS (Eq. S2) and using the arithmetic mean value and the Measurement error (*M.e.*) of the repeated determinations (Eq. S3).

$$\mathrm{n(Prod.)} = \frac{\int \mathrm{Prod.} \cdot \mathrm{n(TMSS)} \cdot \mathrm{N(TMSS)}}{\mathrm{N(Prod.)} \cdot \int \mathrm{TMSS}} \qquad \textbf{Eq. S2}$$

The values of *M.e.* are used as error bars of the data of x in the plots (x = concentration, n = number of samples).

$$M.e. = \sqrt{\frac{\sum(\mathrm{x}-\bar{\mathrm{x}})^2}{\mathrm{n}}} \qquad \textbf{Eq. S3}$$

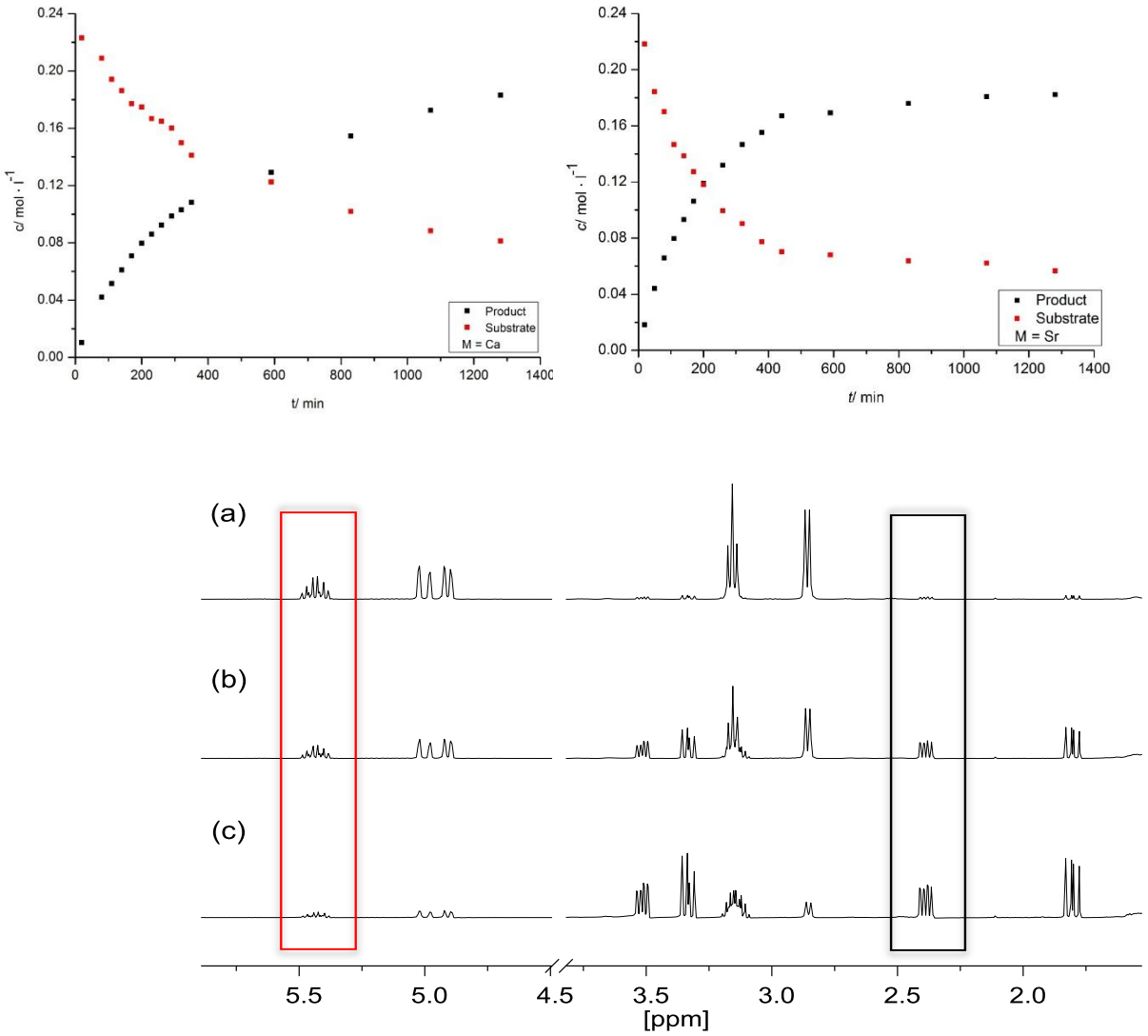

Figure S4. Intramolecular hydroamination of 2,2-diphenyl-pent-4-enylamine (top) was monitored by ^{1}H NMR spectroscopy in the presence of 3 mol% precatalyst **2c** (top left) and **3c** (top right) in C_6D_6. Conversion to the heterocyclic product was followed by integration of the resonances of the substrate and the product in the ^{1}H NMR spectra relative to an internal TMSS standard (exemplified in Table S2). Exemplary NMR spectra (bottom) of the cyclisation of the substrate (red) to the pyrrolidine derivative (black) using 3 mol-% **2c** after 20 min (a), 200 min (b) and 1070 min (c) at r.t. are depicted.

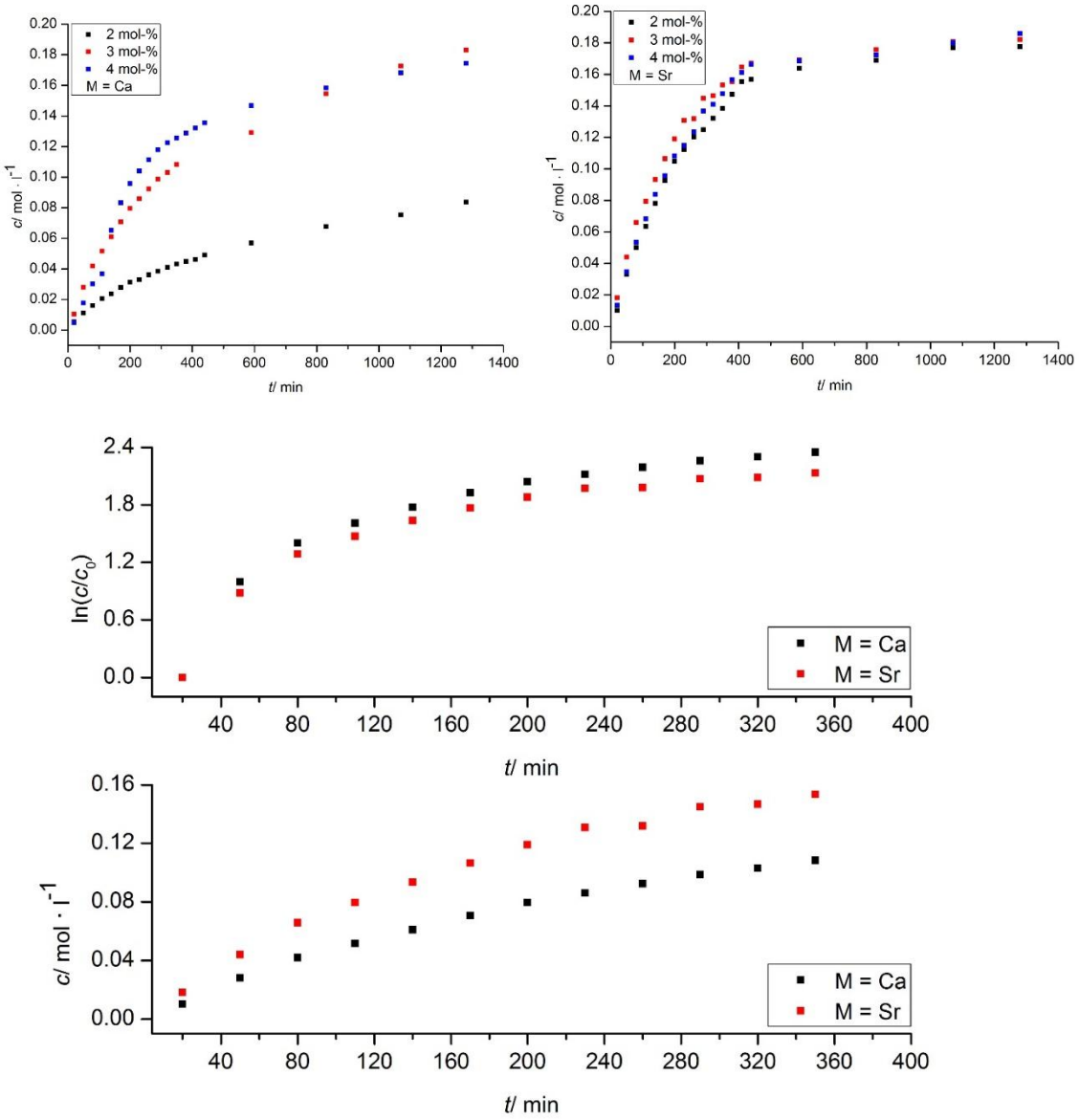

Figure S5.To determine the rate law kinetics, analyses were performed repeatedly at three different catalyst loadings (2, 3, and 4 mol-%). Reaction rates k (min^{-1}) were derived from the slopes of the plot of [product] versus time. Zero order reaction kinetics show the best fits under the condition that the concentration of the substrate is much smaller than the concentration of the product (i.e. at the beginning of the metal-mediated catalytic hydroamination):

[2,2-diphenyl-pent-4-enylamine] ≥ [2-methyl-4,4-diphenylpyrrolidine].

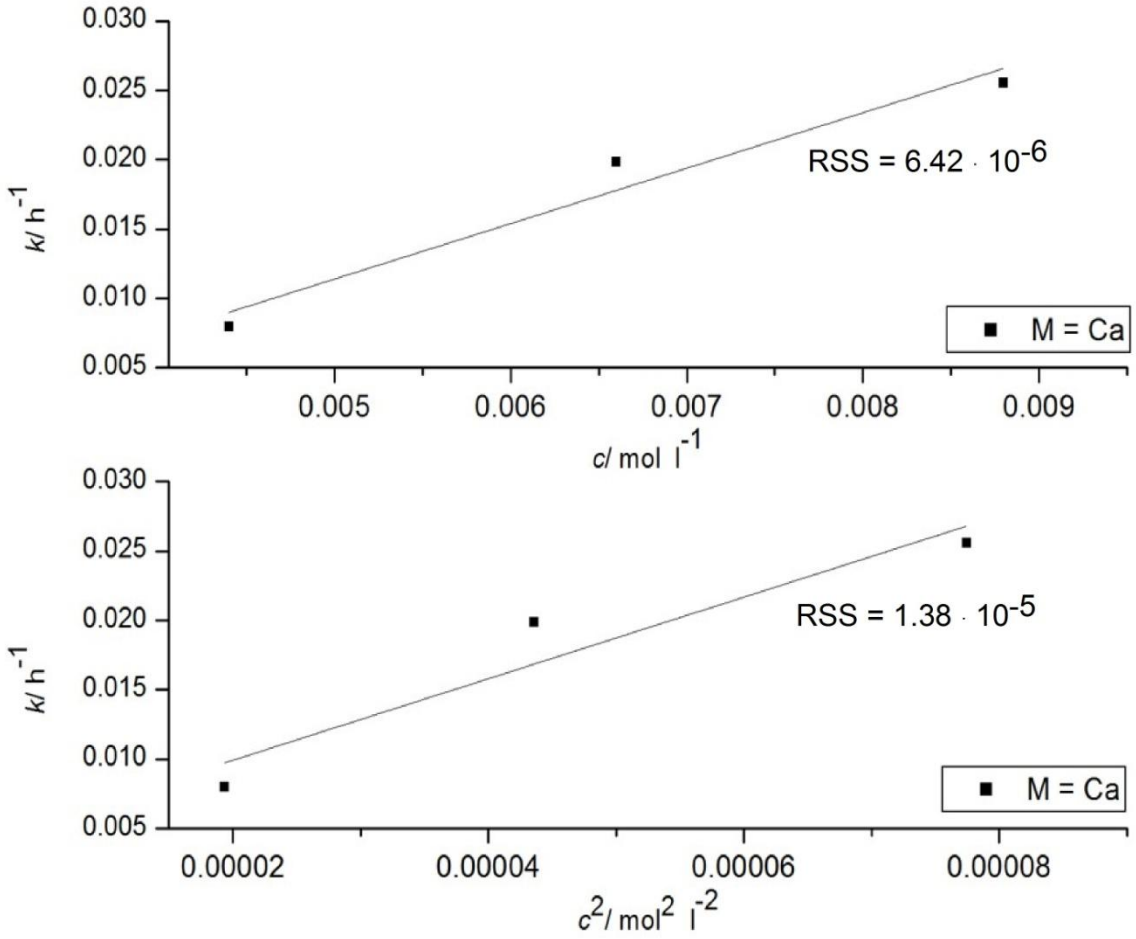

Figure S6. Plots of reaction rate as functions of catalyst concentration and squared catalyst concentrationat at room temperature. The residual sum of squares (RSS) is used as rate of the deviation from the linearity.

The data best fit to a first-order dependence upon catalyst concentration and implicate a rate-determining step involving the precatalyst metal center. The residual sum of squares (RSS) is only slightly lower in the case of first-order than in second-order dependence, however the rate law can described as:

$$rate = k[aminoalkene]^0[catalyst]^1 \qquad \textbf{Eq. S4}$$

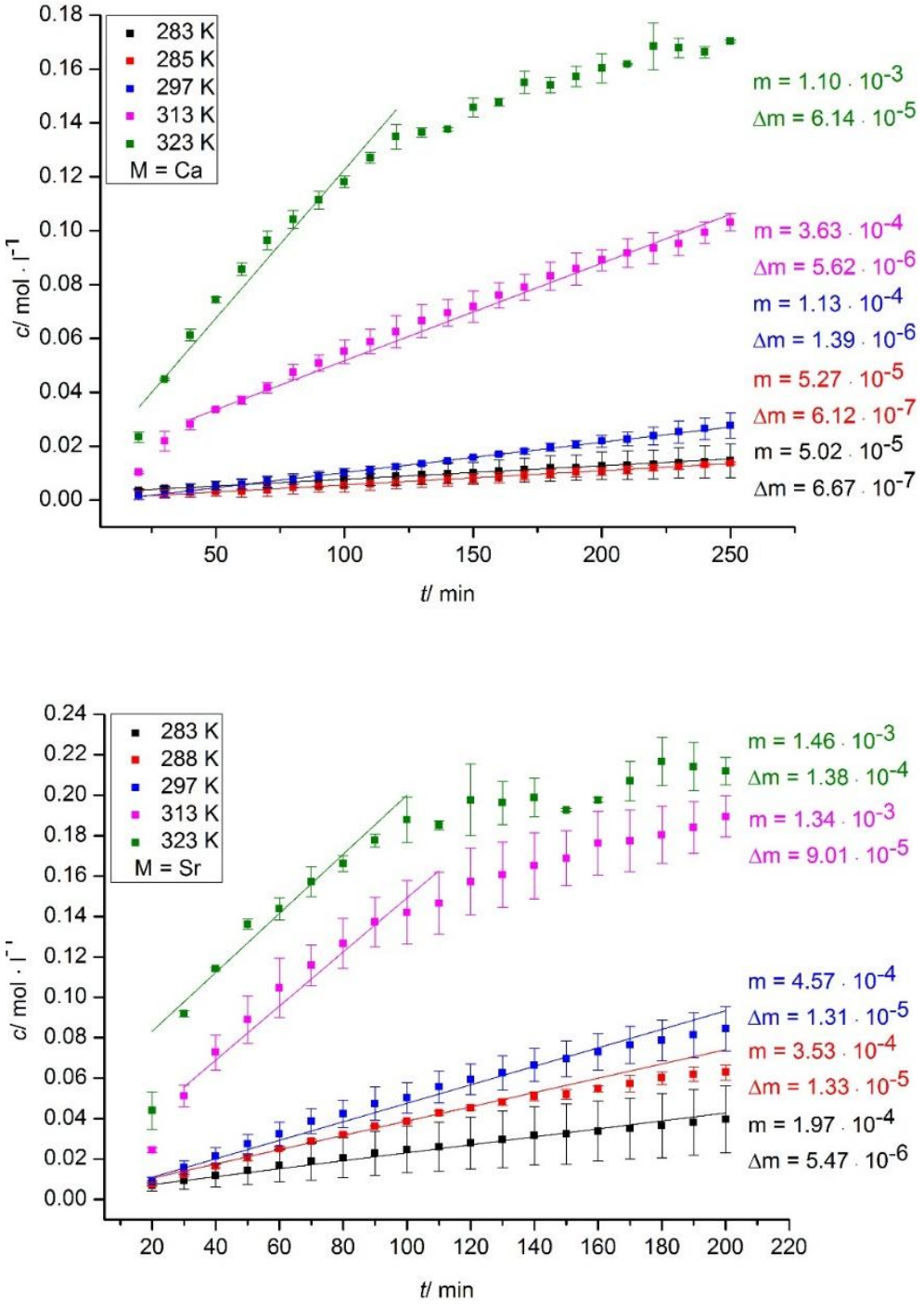

Figure S7. To obtain Arrhenius and Eyring plots, kinetic analyses were conducted at 5 different temperatures as shown in the inset (3 mol-% of precatalyst **2c** (top) and **3c** (bottom) were used). The rates increase with temperature and *M.e.* values are used to determine the weighted sum of reaction rates k at different temperatures.

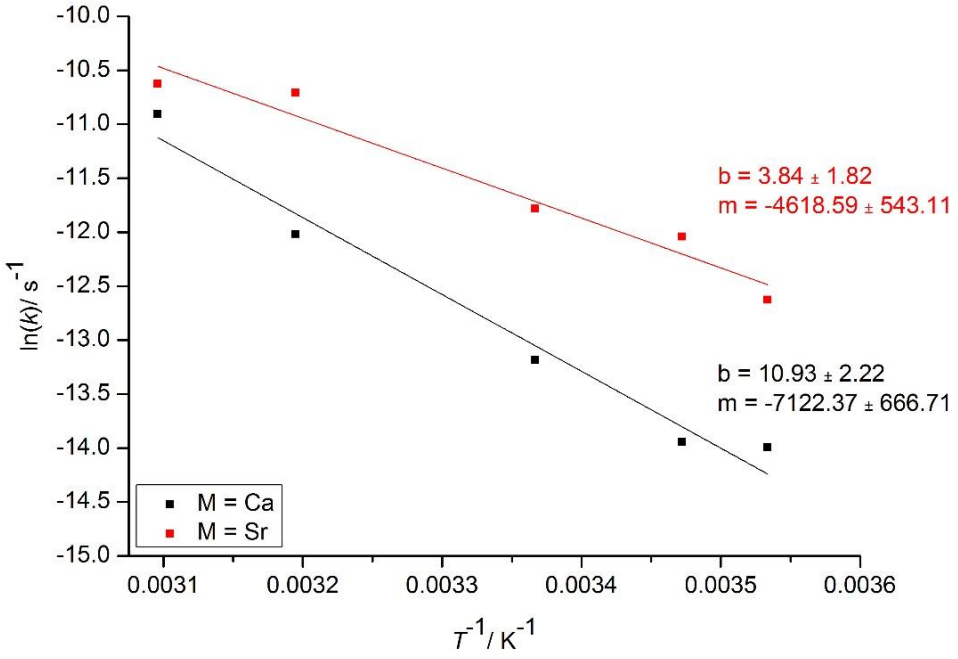

Figure S8. Standard Arrhenius analyses provided activation energies E_a.

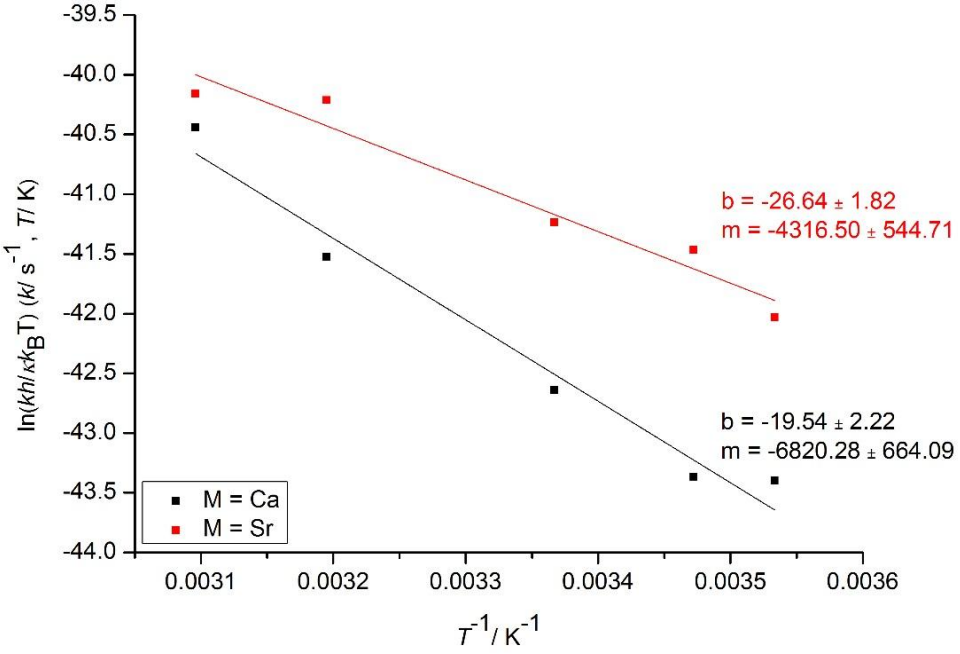

Figure S9. The Eyring analyses provided values to describe the transitional state

Activation energies derived from Arrhenius equation:

$$k = A \cdot e^{-\frac{E_a}{RT}} \implies \ln(k) = \ln(A) - \frac{E_a}{RT} \quad \textbf{Eq. S5}$$

Transitional state parameters derived from Eyring equation:

$$\ln\left(\frac{k \cdot h}{k_B \cdot T}\right) = -\frac{\Delta H^{\ddagger}}{RT} + \frac{\Delta S^{\ddagger}}{R} \quad \textbf{Eq. S6}$$

Used natural constants:

R = 8,31445985 J·mol^{-1}·K^{-1}, h = 6.626068·10^{-34} J·s, k_B = 1.3806503·10^{-23} J·K^{-1}

k = reaction rate in s^{-1} and T = absolute temperature in K

Catalytic parameters derived from Eqs. S7–S9 (t = 16 h).

$$\tau_{1/2} = \frac{[\text{Subs.}]_{t=0}}{2 \cdot k} \quad \textbf{Eq. S7}$$

$$\text{TON} = \frac{[\text{Prod.}]_t}{[\text{Cat.}]_{t=0}} \quad \textbf{Eq. S8}$$

$$\text{TOF} = \frac{k}{[\text{Cat.}]_{t=0}} \quad \textbf{Eq. S9}$$

All values to describe the catalytic activities are summarized in Table 1.

Table S1. Catalytic parameters derived from kinetic, Arrhenius and Eyring analyses.

	Conv. [%] after 16 h	k [h^{-1}]	$\tau_{1/2}$ [h]	TON	TOF [h^{-1}]
2 mol-% Ca	38	0.008	15	19	1.8
3 mol-% Ca	77	0.020	6	29	3.0
4 mol-% Ca	73	0.026	5	20	2.9
2 mol-% Sr	80	0.022	5	49	5.1
3 mo-l% Sr	82	0.029	4	31	4.4
4 mol-% Sr	82	0.026	5	25	3.0

	A [s^{-1}]	E_a [kJ·mol^{-1}]	$\Delta H^{\ddagger}$ [kJ·mol^{-1}]	$\Delta S^{\ddagger}$ [J·mol^{-1}·K^{-1}]	$\Delta G^{\ddagger}$ [kJ·mol^{-1}] (r.t.)
3 mol% Ca	10367 ± 5	59 ± 6	57 ± 6	-163 ± 18	105 ± 5
3 mol% Sr	50 ± 7	38 ± 5	36 ± 5	-221 ± 15	102 ± 4

NMR spectra

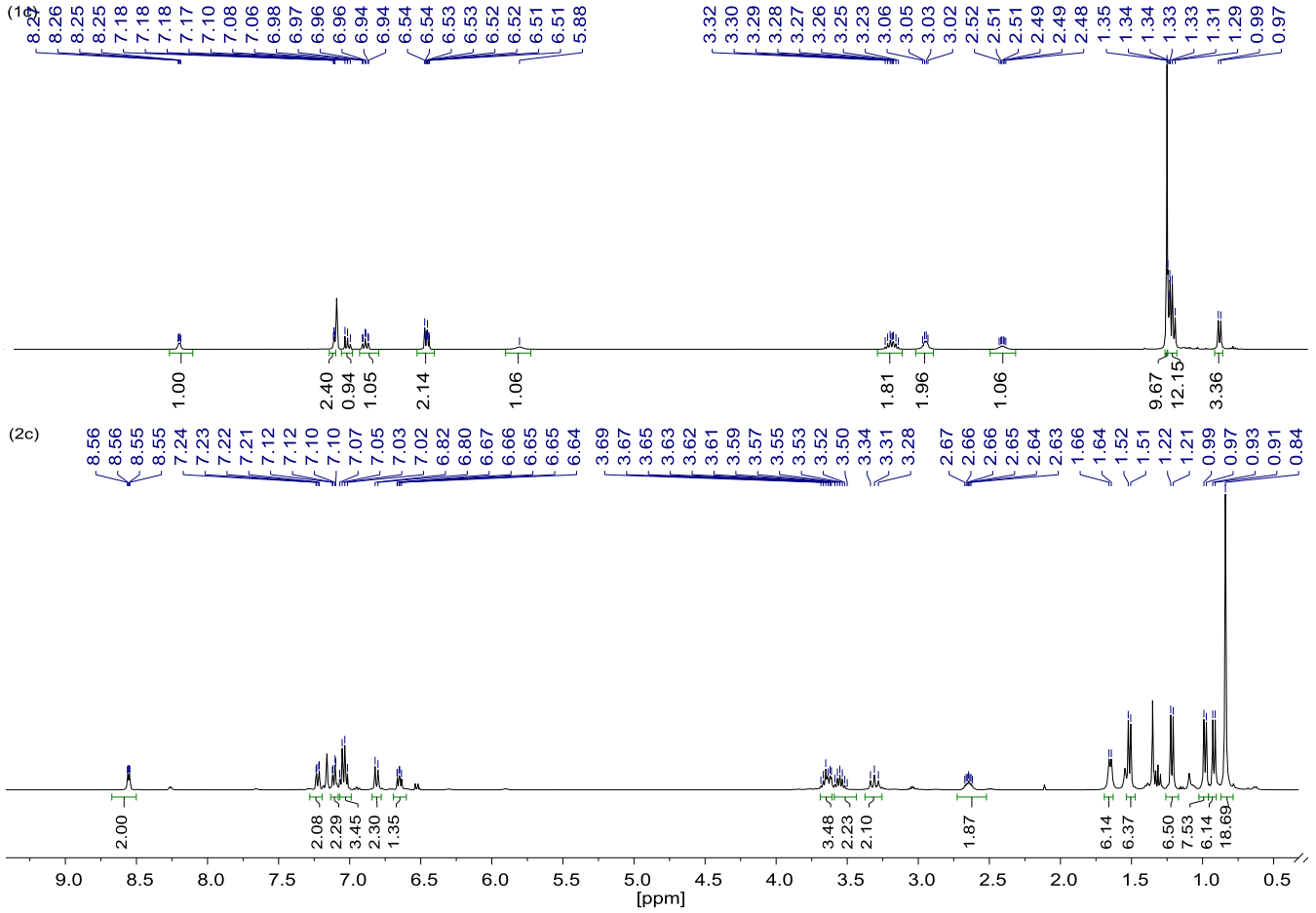

Figure S10. ^{1}H NMR spectra of Dipp−N=C(tBu)−N(H)−$CH_2CH(CH_3)$−Py (**1d**, top, C_6D_6, 297.0 K, 400.13 MHz); [Ca{Dipp−N=C(tBu)N−$CH_2CH(CH_3)$−Py}$_2$] (**2d**, bottom, C_6D_6, 297.0 K, 400.22 MHz).

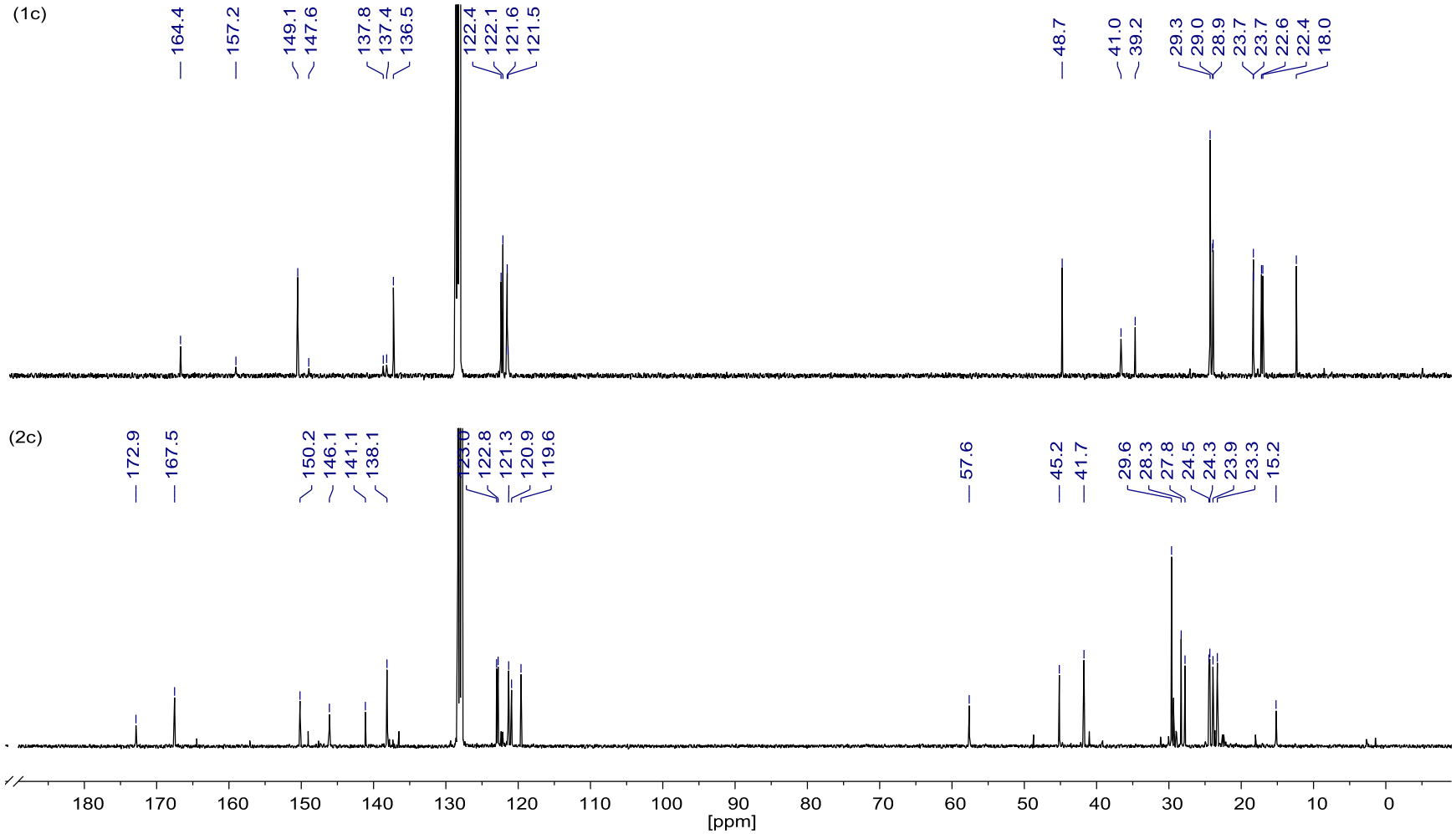

Figure S11. $^{13}C\{^{1}H\}$ NMR spectra of Dipp−N=C(tBu)−N(H)−$CH_2CH(CH_3)$−Py (**1d**, top, C_6D_6, 297.0 K, 100.62 MHz); [Ca{Dipp−N=C(tBu)N−$CH_2CH(CH_3)$−Py}$_2$] (**2d**, bottom, C_6D_6, 297.0 K, 100.65 MHz).

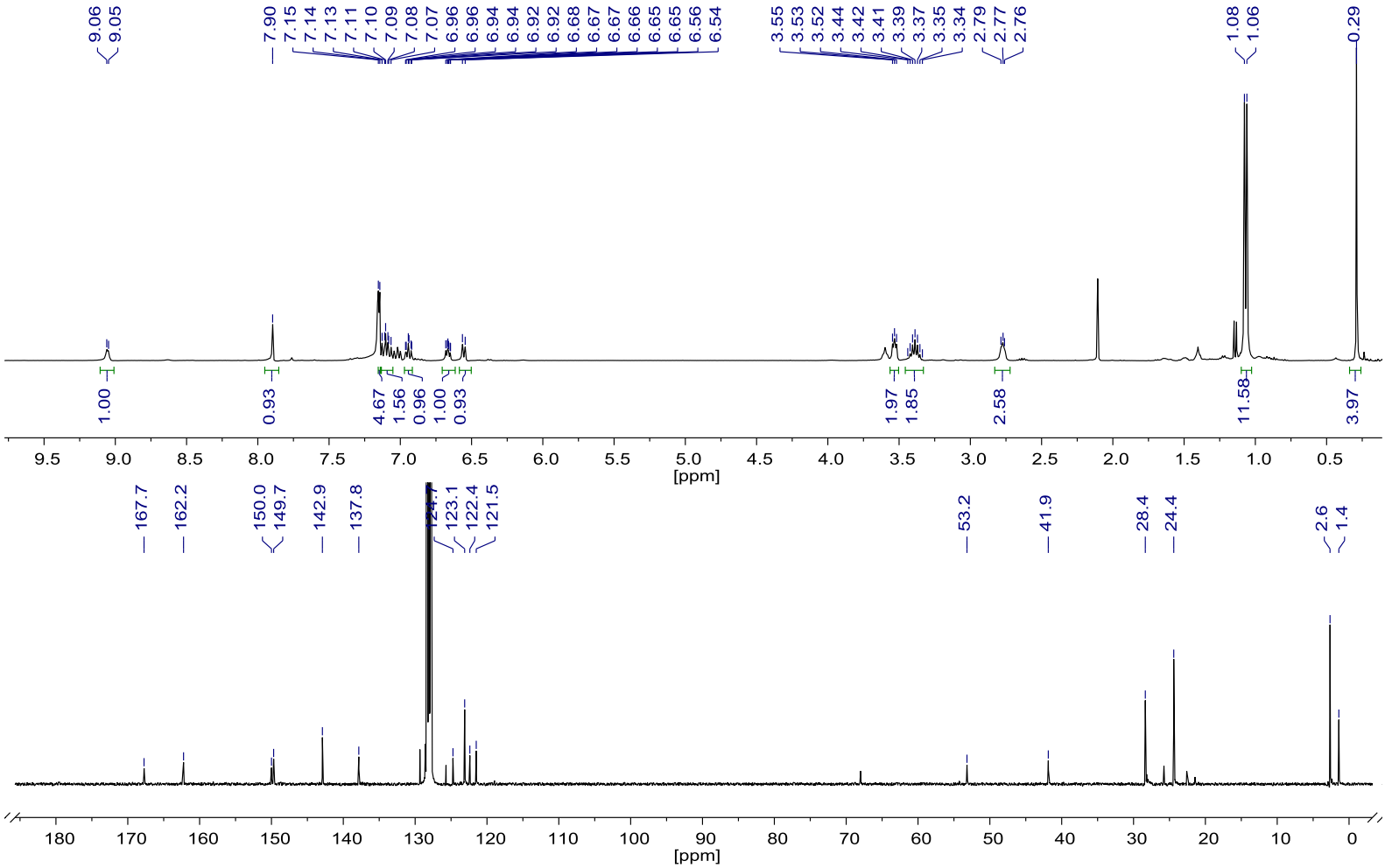

Figure S12. ^{1}H NMR (top, C_6D_6, 297.0 K, 400.22 MHz) and $^{13}C\{^{1}H\}$ NMR (bottom, C_6D_6, 297.0 K, 100.63 MHz) spectra of $[\{(Me_3Si)_2N\}Ca\{Dipp{-}N{=}C(H)N{-}C_2H_4{-}Py\}]_2$ (**2a**) after rearrangement to $[Ca\{Dipp{-}N{=}C(H)N{-}C_2H_4{-}Py\}_2]$.

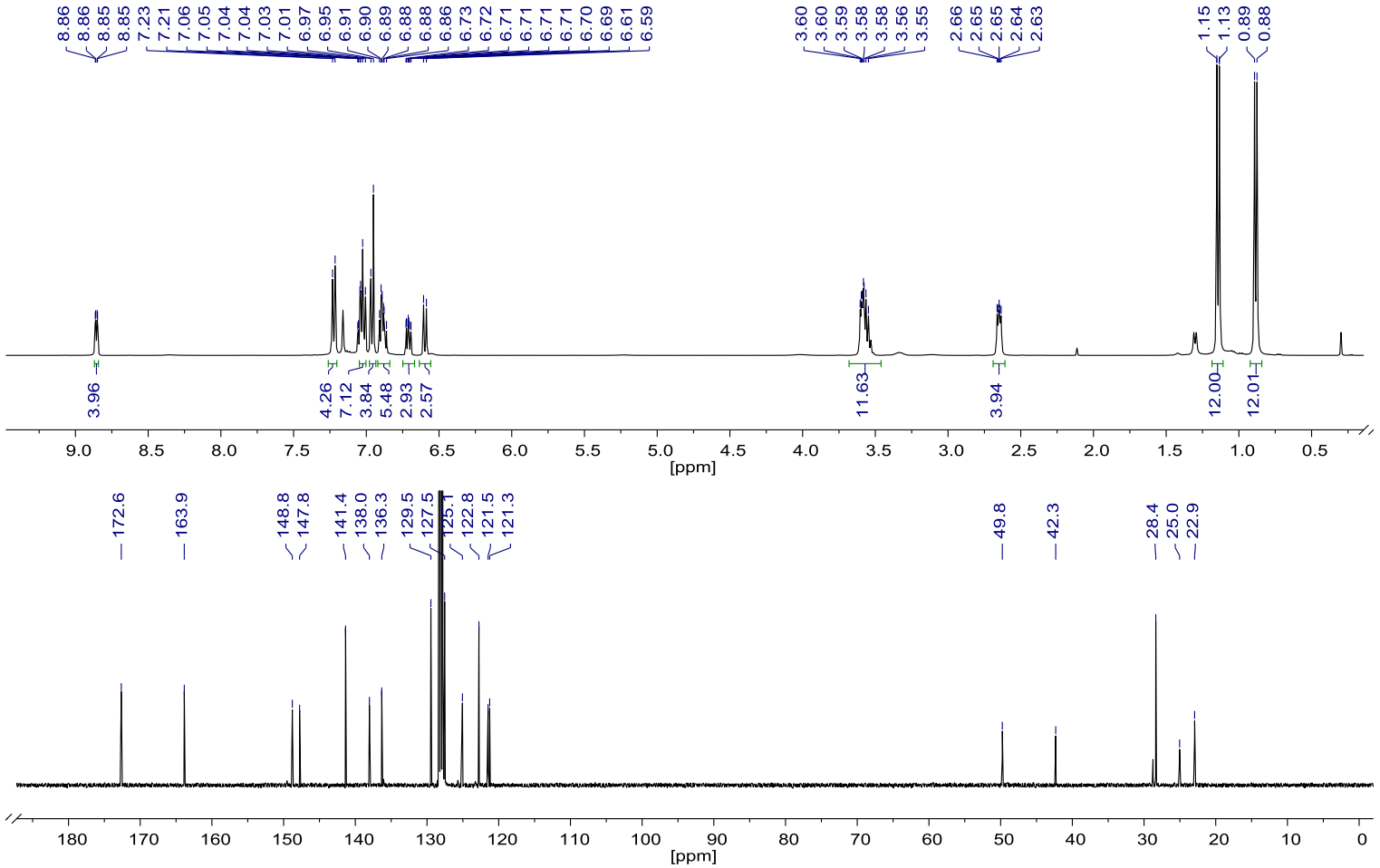

Figure S13. ^{1}H NMR (top, C_6D_6, 297.0 K, 400.13 MHz) and $^{13}C\{^{1}H\}$ NMR (bottom, C_6D_6, 297.0 K, 100.61 MHz) spectra of [Ca{Dipp−N=C(Ph)N−C_2H_4−Py}$_2$] (**2b**).

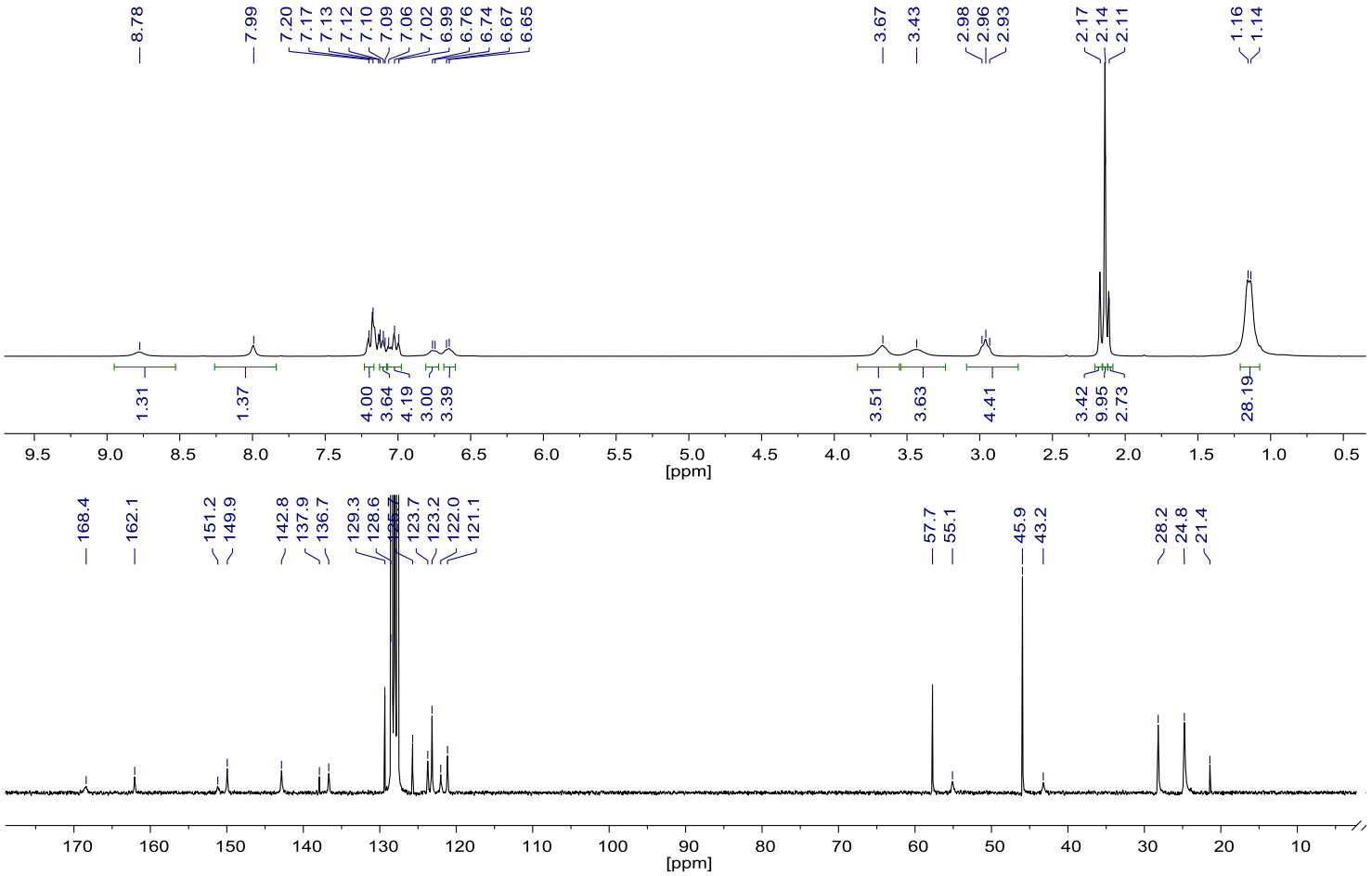

Figure S14. ^{1}H NMR (top, C_6D_6, 296.9 K, 250.13 MHz) and $^{13}C\{^{1}H\}$ NMR (bottom, C_6D_6, 296.9 K, 62.90 MHz) spectra of [(tmeda)Sr{Dipp−N=C(H)N−C_2H_4−Py}$_2$] (**3a**).

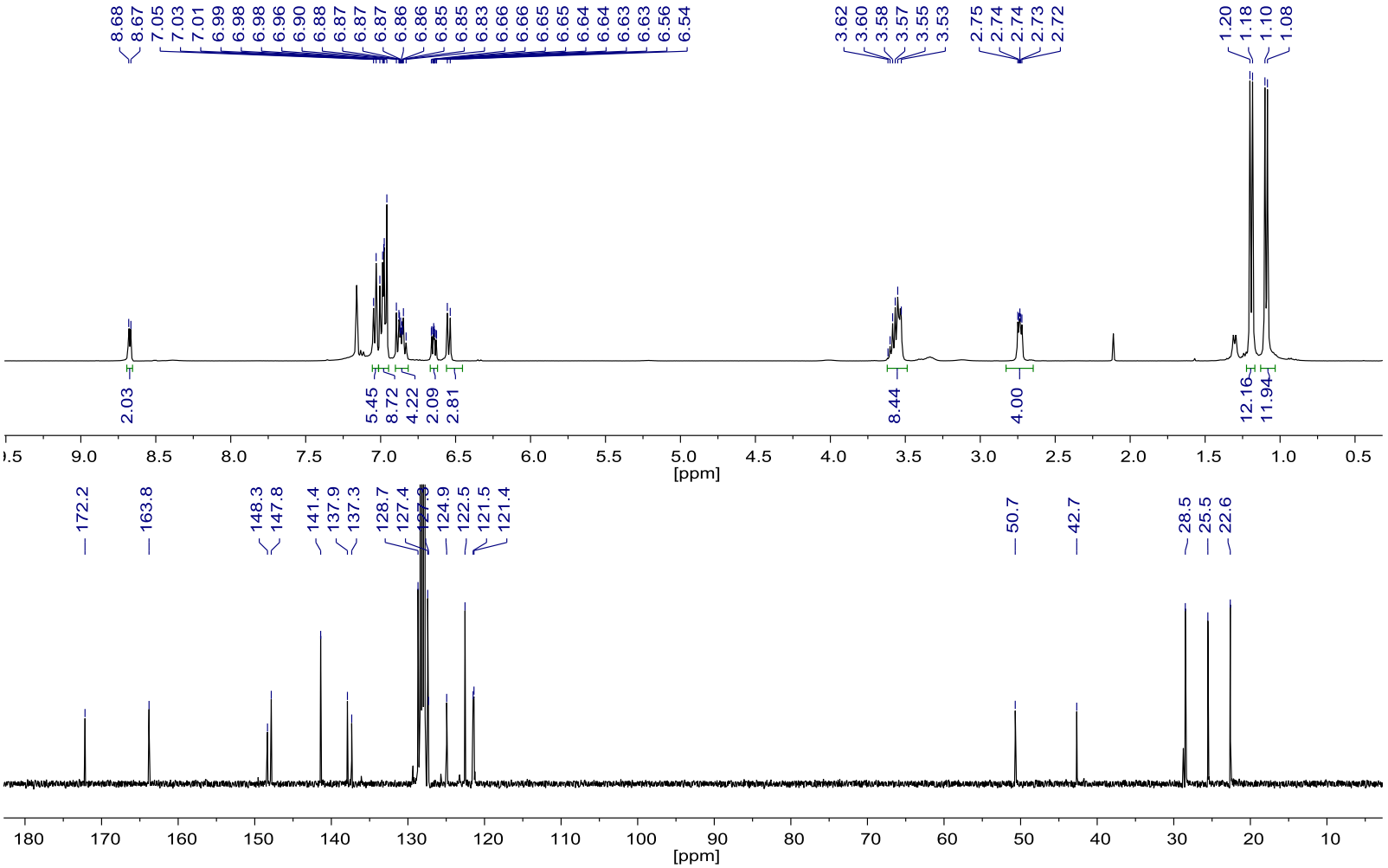

Figure S15. ^{1}H NMR (top, C_6D_6, 297.0 K, 400.13 MHz) and $^{13}C\{^{1}H\}$ NMR (bottom, C_6D_6, 297.0 K, 100.61 MHz) spectra of [Sr{Dipp−N=C(Ph)N−C_2H_4−Py}$_2$] (**3b**).

Table S2: Crystal data and refinement details for the X-ray structure determinations of the compounds **2a'** - ***(R,R)*-2d**.

Compound	**2a'**	**2b**	***(R,R)*-2d**
formula	$C_{52}H_{88}Ca_2N_8Si_4$[*]	$C_{52}H_{60}CaN_6$	$C_{50}H_{72}CaN_6$
fw ($g \cdot mol^{-1}$)	1017.82[*]	809.14	797.22
°C	-140(2)	-140(2)	-140(2)
crystal system	Monoclinic	monoclinic	monoclinic
space group	P 2_1/c	P 2_1/n	P 2_1
a/ Å	11.7902(2)	11.9432(2)	11.9581(2)
b/ Å	27.3841(6)	19.2797(3)	16.9041(3)
c/ Å	11.3666(2)	20.0270(4)	12.7267(2)
α/°	90	90	90
β/°	90.675(1)	95.972(1)	114.685(1)
γ/°	90	90	90
V/Å^3	3669.61(12)	4586.42(14)	2337.50(7)
Z	2	4	2
ρ ($g \cdot cm^{-3}$)	0.921[*]	1.172	1.133
μ (cm^{-1})	2.52[*]	1.78	1.73
measured data	25649	29604	27728
data with I > 2σ(I)	6602	6860	9730
unique data (R_{int})	8348/0.0385	10453/0.1048	10305/0.0272
wR_2 (all data, on F^2)[a)]	0.1476	0.1804	0.0841
R_1 ($I > 2\sigma(I)$) [a)]	0.0558	0.0799	0.0374
s[b)]	1.080	1.129	1.042
Res. dens./$e \cdot Å^{-3}$	0.439/-0.383	0.396/-0.322	0.618/-0.198
Flack-parameter	-	-	0.02(2)
absorpt method	multi-scan	multi-scan	multi-scan
absorpt corr $T_{min}/_{max}$	0.7013/0.7456	0.5355/0.7456	0.7175/0.7456
CCDC No.	1884727	1884728	1884729

[*] derived parameters do not contain the contribution of the disordered solvent.

contd. Table S2: Crystal data and refinement details for the X-ray structure determinations of the compounds ***(S,S)*-2d - 3b**.

Compound	***(S,S)*-2d**	**3a**	**3b**
formula	$C_{50}H_{72}CaN_6$	$C_{53}H_{76}N_8Sr$	$C_{52}H_{60}N_6Sr$
fw ($g \cdot mol^{-1}$)	797.22	912.84	856.68
°C	-140(2)	-140(2)	-140(2)
crystal system	monoclinic	monoclinic	monoclinic
space group	P 2_1	P $2_1/c$	P $2_1/n$
a/ Å	11.9728(2)	13.7474(3)	11.8846(2)
b/ Å	16.9256(4)	27.3642(5)	19.3809(2)
c/ Å	12.7315(3)	14.5119(2)	20.1264(3)
α/°	90	90	90
β/°	114.750(1)	110.447(1)	95.693(1)
γ/°	90	90	90
V/Å^3	2343.01(9)	5115.23(16)	4612.93(11)
Z	2	4	4
ρ ($g \cdot cm^{-3}$)	1.130	1.185	1.234
μ (cm^{-1})	1.73	10.96	12.1
measured data	24162	53430	27257
data with I > 2σ(I)	9692	9605	8015
unique data (R_{int})	10536/0.0308	11669/0.0390	10151/0.0481
wR_2 (all data, on F^2)[a)]	0.0875	0.0894	0.0867
R_1 ($I > 2\sigma(I)$) [a)]	0.0404	0.0433	0.0460
s[b)]	1.071	1.078	1.123
Res. dens./$e \cdot Å^{-3}$	0.407/-0.203	0.717/-0.550	0.438/-0.425
Flack-parameter	0.01(2)	-	-
absorpt method	multi-scan	multi-scan	multi-scan
absorpt corr $T_{min}/_{max}$	0.6823/0.7456	0.6798/0.7456	0.6054/0.7456
CCDC No.	1884730	1884731	188472732

[a)] Definition of the *R* indices: $R_1 = (\Sigma \, || F_o | - | F_c ||) / \Sigma | F_o |$;
$wR_2 = \{\Sigma[w(F_o^2 - F_c^2)^2] / \Sigma[w(F_o^2)^2]\}^{1/2}$ with $w^{-1} = \sigma^2(F_o^2) + (aP)^2 + bP$; $P = [2F_c^2 + Max(F_O^2]/3$;
[b)] $s = \{\Sigma[w(F_o^2 - F_c^2)^2] / (N_o - N_p)\}^{1/2}$.

Molecular representations

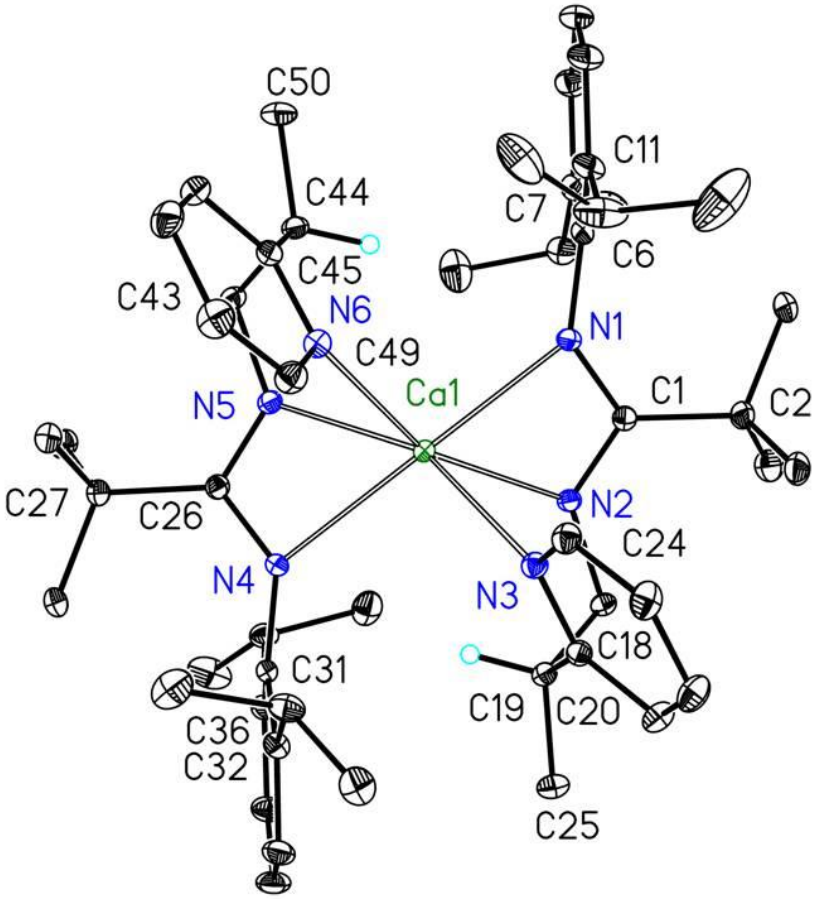

Figure S16. Molecular structure and numbering scheme of [Ca{Dipp−N=C(*t*Bu)-N−$CH_2CH(CH_3)$−Py}$_2$] *(R,R)*-**2d**. The ellipsoids represent a probability of 30 %, hydrogen atoms are neglected for the sake of clarity.

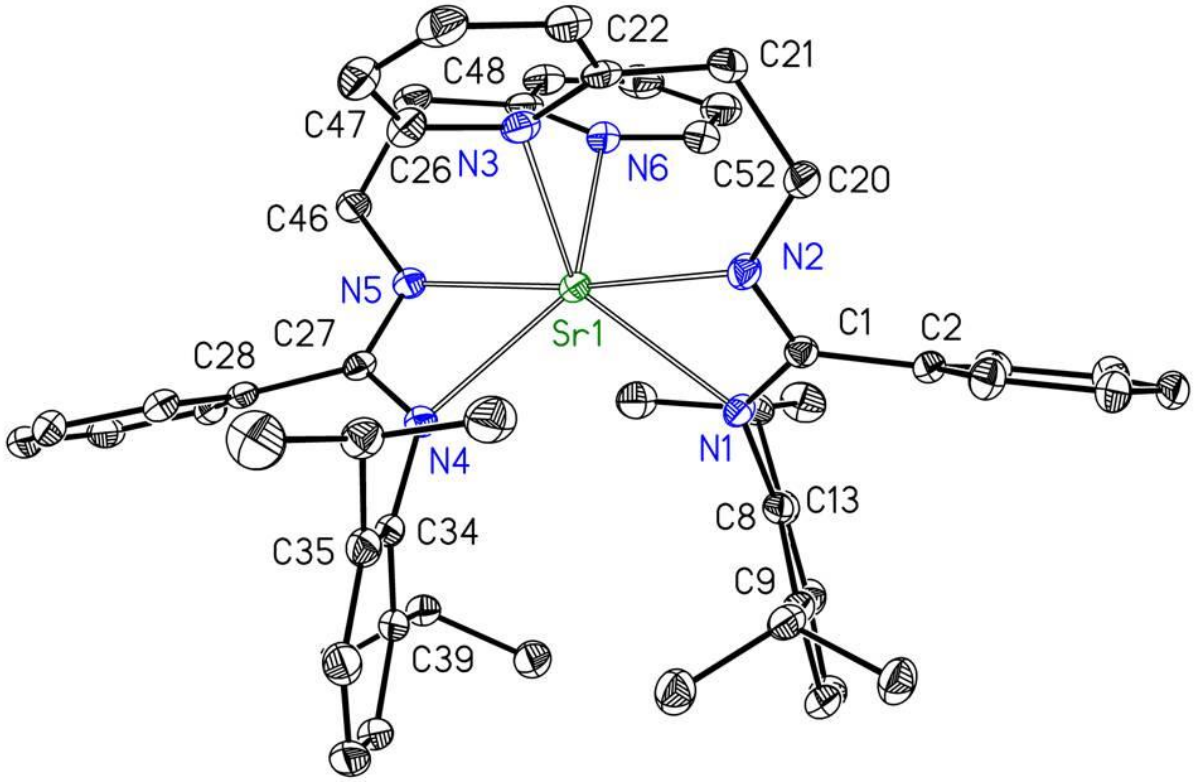

Figure S17. Molecular structure and numbering scheme of [Sr{Dipp−N=C(Ph)-N−C_2H_4−Py}$_2$] (**3b**). The ellipsoids represent a probability of 30 %, hydrogen atoms are omitted for clarity reasons.

References

[1] Martínez, P. H.; Hultzsch, K. C.; Hampel, F. *Chem. Commun.* **2006**, 2221–2223.

[2] Kalden, D.; Oberheide, A.; Loh, C.; Görls, H.; Krieck, S.; Westerhausen, M. *Chem. Eur. J.* **2016**, *22*, 10944–10959.